INTERNATIONAL JOURNAL FOR NUMERICAL METHODS IN FLUIDS, VOL. 7, 1147–1158 (1987)

EXPLICIT ADAPTIVE CALCULATIONS OF WRINKLED FLAME PROPAGATION*

F. BENKHALDOUN AND B. LARROUTUROU

INRIA, Sophia-Antipolis, F-06560 Valbonne, France

SUMMARY

The aim of this work is to study the propagation of a curved premixed flame in an infinite two-dimensional tube. The numerical method combines some features of the finite-element and of the finite-difference methods, and uses a moving adaptive grid procedure in order to reduce the computational costs.

KEY WORDS Flame Propagation Reaction–Diffusion System Finite Elements Adaptive Grid

INTRODUCTION

This paper is devoted to the numerical solution of the classical thermal diffusional model describing the propagation of a wrinkled flame front in a gaseous mixture. This non-linear reaction diffusion model is a simplified system of governing equations, but its numerical investigation presents many interesting features for numerical analysts.

In particular, in most gaseous combustion phenomena, the chemical reaction rates exhibit a very strong non-linear dependence with respect to the temperature. Because of this dependence, disparate time and space scales appear in the physical phenomenon, and the resulting partial differential equations are stiff. To be more specific, a flame propagation phenomenon presents a very narrow zone of sharp gradients, the flame front, dividing two regions in which the variables are almost constant. Moreover, the reaction rates (which determine the flame speed and the overall burning rate of the mixture) appear to be non-negligible only in a thin layer within the flame front. For these reasons, an *adaptive grid* is required for a proper simulation of the flame propagation, in order to solve accurately the small length scales while avoiding the use of a dense mesh in the regions of no particular interest.

Thus we will be led to solve reactive–diffusive partial differential equations in a rectangle using a highly non-uniform two-dimensional grid. This will be done with a spatial approximation scheme which combines some features of the classical finite-element and finite-difference methodologies, because of the robustness of the former for the approximation of diffusive terms on irregular meshes, and of the simplicity of the latter for problems posed in a geometrically simple domain.

The paper is organized as follows: we first state the mixed initial-boundary value problem under consideration; we next present in detail the discrete scheme and the adaptive mesh strategy used for its numerical solution; we finally illustrate the ability of the method to compute wrinkled flame fronts by showing some numerical results corresponding to two different physical situations.

* Based on a contributed paper

0271–2091/87/111147–12$06.00

FORMULATION OF THE PROBLEM

The thermo-diffusive model

The analysis of the unsteady propagation of a wrinkled flame front in a gaseous mixture is a strongly non-linear problem involving the classical complexity of non-reacting gas flows coupled with the effects of thermal conduction and molecular diffusion and with a (possibly complex) mechanism of chemical reactions. The description of this phenomenon with a numerically or analytically tractable system of governing equations often uses some simplifications, such as the *isobaric approximation*, which consists of neglecting the effects of the mixture compressibility and therefore eliminates the acoustic waves, or the *constant-density approximation*, which uncouples the flame propagation itself from the gas flow, but retains many essential features of the phenomenon, including the cellular instabilities of the flame.[1-3] The constant-density approximation therefore seems physically relevant for qualitatively describing combustion phenomena in which the gas motion is almost uniform and plays a secondary role compared with the reactive and diffusive effects. In this constant-density model, which is also known as the *thermo-diffusive model*, the flame propagation is simply described by a non-linear system of reaction–diffusion equations (equations (1) below).

We will consider in this paper the propagation of a wrinkled flame in a rectangular channel, represented by the semi-infinite domain $\{(x, y),\ -R \leqslant y \leqslant R\}$. Assuming for simplicity that a single one-step chemical reaction $A \rightarrow B$ takes place in the gaseous mixture and using the constant-density approximation, we use the following system of governing equations:

$$T_t = \Delta T + \Omega(Y, T), \quad Y_t = \frac{1}{\mathrm{Le}} \Delta Y - \Omega(Y, T). \tag{1}$$

These equations are written using normalized variables: T is the reduced temperature of the mixture, Y is the mass fraction of the reactant A and Ω is the normalized reaction rate, given by

$$\Omega(Y, T) = \frac{\beta^2}{2\mathrm{Le}} Y \exp\left(- \frac{\beta(1-T)}{1-\alpha(1-T)} \right),$$

where $\beta > 0$ denotes the reduced activation energy of the chemical reaction, $\mathrm{Le} > 0$ is the Lewis number of the reactant and $\alpha \in (0, 1)$ is a non-dimensional heat release parameter (see References 4 and 5 for more details about the non-dimensionalization of these equations). The initial and boundary conditions associated with equations (1) are

$$T(t=0) \equiv T_0, \quad Y(t=0) \equiv Y_0, \tag{2}$$

$$T = 0, \quad Y = 1 \quad \text{for } x = -\infty, \tag{3a}$$

$$T = 1, \quad Y = 0 \quad \text{for } x = +\infty, \tag{3b}$$

$$\frac{\partial T}{\partial y} = 0, \quad \frac{\partial Y}{\partial y} = 0 \quad \text{for } y = \pm R \tag{3c}$$

when the flame is propagating in a channel with adiabatic walls. (In the case of a non-adiabatic propagation, the conditions (3b) at the hot boundary and the conditions (3c) at the tube walls are modified; see the Numerical results section.)

Problem in a bounded domain

The numerical investigation of the above problem (1)–(3) of course requires the formulation

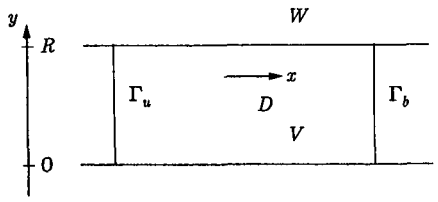

Figure 1. The computational domain D

of an analogous problem posed in a bounded domain. We now state this approximate problem to be solved numerically.

Seeking only solutions symmetric with respect to the channel axis $y = 0$, we restrict the numerical study to the upper half of the tube. The computational domain is therefore a rectangular portion $D = [a, b] \times [0, R]$ of the infinite tube, as shown in Figure 1.

The problem to be solved on the computational domain D consists of the equations (1) with the initial data (2) and the following boundary conditions:

$$\frac{\partial T}{\partial n} = 0, \quad \frac{\partial Y}{\partial n} = 0 \quad \text{on} \quad W, \tag{4a}$$

$$\frac{\partial T}{\partial n} = 0, \quad \frac{\partial Y}{\partial n} = 0 \quad \text{on} \quad V \quad \text{(symmetry condition)}, \tag{4b}$$

$$T = 0, \quad Y = 1 \quad \text{on} \quad \Gamma_u, \tag{4c}$$

$$T = 1, \quad Y = 0 \quad \text{on} \quad \Gamma_b. \tag{4d}$$

Remark 1. If the boundaries Γ_u and Γ_b are far enough from the flame front, which is required for an accurate computation, the Dirichlet conditions (4c)–(4d) on these boundaries may be replaced by homogeneous Neumann conditions $\partial T/\partial x = \partial Y/\partial x = 0$ on Γ_u and Γ_b. Such a modification of the boundary conditions scarcely influences the solution in the case of a stable adiabatic flame propagation, but is necessary for a non-adiabatic problem (see the Numerical results section).

NUMERICAL APPROXIMATION

Spatial approximation

As pointed out in the Introduction, the numerical solution of the problem (1)–(4) will be sought using an adaptive mesh. Our discrete approximation therefore needs to be robust and usable even on highly non-uniform grids. This will be attained by combining some features of the classical finite-difference and finite-element approximations.

To be more specific, let Θ_h be a finite-element triangulation of the computational domain D (in the usual sense; see Reference 6). We introduce classical P1 Lagrange triangular finite elements with the discretization spaces

$$V_h = \{v \in C^0(D), \forall\, T \in \Theta_h, v|_T \in P_1\},$$

$$V_h^0 = \{v \in V_h, v = 0 \quad \text{on} \quad \Gamma_u \cup \Gamma_b\}.$$

Let Σ be the set of vertices of the triangulation Θ_h and $\Sigma_u = \Sigma \cap \Gamma_u$, $\Sigma_b = \Sigma \cap \Gamma_b$. We define the sets of indices I, I_u, I_b and I^0 by setting $\Sigma = \{N_i,\ i \in I\}$, $\Sigma_u = \{N_i,\ i \in I_u\}$,

$\Sigma_b = \{N_i,\ i \in I_b\}$, $I^0 = I - (I_u \cup I_b)$. Finally, let $(\varphi_i)_{i\in I}$ be the classical basis of the finite-dimensional space $V_h((\varphi_i)_{i\in I^0}$ is a basis of V_h^0). A straightforward finite-element approximation of the problem (1)–(4) leads to the following (spatially discretized) problem:

find $T_h = \sum_{i\in I^0} T_i(t)\varphi_i + \sum_{i\in I_b} \varphi_i$ and $Y_h = \sum_{i\in I^0} Y_i(t)\varphi_i + \sum_{i\in I_u} \varphi_i$ such that

$$\int_D \left(\sum_{i\in I^0} \frac{dT_i}{dt} \varphi_i \right) \varphi_j = -\int_D \left(\sum_{i\in I} T_i \nabla\varphi_i \right) \nabla\varphi_j + \int_D \Omega(Y_h, T_h)\varphi_j, \tag{5}$$

$$\int_D \left(\sum_{i\in I^0} \frac{dY_i}{dt} \varphi_i \right) \varphi_j = -\frac{1}{\mathrm{Le}} \int_D \left(\sum_{i\in I} Y_i \nabla\varphi_i \right) \nabla\varphi_j - \int_D \Omega(Y_h, T_h)\varphi_j, \quad \forall j \in I^0.$$

Unfortunately, the mass matrix $[M_{ij}] = [\int_D \varphi_j \varphi_i]$ which appears in the left-hand side of the above equations is not diagonal (which prevents us from using an explicit time integration method) and does not satisfy the maximum principle (i.e. the inequality $M_{ij}^{-1} \geqslant 0$ does not hold for all i and j). In order to avoid these difficulties, we employ instead of (5) the mass lumped approximation of (5),

$$\frac{dT_j}{dt} \int_D \varphi_j = -\int_D \left(\sum_{i\in I} T_i \nabla\varphi_i \right) \nabla\varphi_j + \Omega_j \int_D \varphi_j,$$

$$\frac{dY_j}{dt} \int_D \varphi_j = -\frac{1}{\mathrm{Le}} \int_D \left(\sum_{i\in I} Y_i \nabla\varphi_i \right) \nabla\varphi_j - \Omega_j \int_D \varphi_j, \quad \forall j \in I^0,$$

which can also be written as

$$\frac{dT_j}{dt} = -\frac{\int_D \left(\sum_{i\in I} T_i \nabla\varphi_i \right) \nabla\varphi_j}{\int_D \varphi_j} + \Omega_j,$$

$$\frac{dY_j}{dt} = -\frac{1}{\mathrm{Le}} \frac{\int_D \left(\sum_{i\in I} Y_i \nabla\varphi_i \right) \nabla\varphi_j}{\int_D \varphi_j} - \Omega_j, \quad \forall j \in I^0. \tag{6}$$

This semi-discrete formulation can therefore be considered as a finite-difference approximation of the governing equation (1): this is exactly true for the time derivative and reactive terms, and

$$-\frac{\int_D \left(\sum_{i\in I} T_i \nabla\varphi_i \right) \nabla\varphi_j}{\int_D \varphi_j}$$

can simply be regarded as a particular finite-difference formula for approximating the Laplacian operator. (If the triangulation Θ_h is obtained from a uniform orthogonal grid, this formula reduces to the usual five-point approximation of ΔT; but it can be hoped to be consistent and robust even on non-uniform meshes.[7]) We refer the reader to Reference 8 for a numerical analysis of the scheme (6) in a finite-difference context.

Time integration

The system of ordinary differential equations (6) is integrated explicitly. Instead of the simple forward Euler scheme, we usually employ a high-order time integration scheme (such as fourth-order Runge–Kutta), because of the stability properties of this scheme for both diffusive and convective terms (the need for dealing with convective terms comes from the moving mesh strategy presented in the next section).

ADAPTIVE MESH STRATEGY

Since the phenomena under study exhibit narrow zones of large gradients (the flame front) separating two regions where all the variables are almost constant (the fresh mixture and the burnt gases), a low-cost numerical description of the propagation requires an adaptive mesh. Moreover, the thin region of high gradients continually moves towards the cold boundary Γ_u. Our mesh adaptation method therefore consists of two different procedures:

(1) the 'dynamic rezone', which is performed at every time step and allows the node locations to vary smoothly with time
(2) the 'static rezone', which is performed only at a few time levels during the calculation in order to redistribute the mesh points better and to adapt still better the grid to the solution.

Dynamic rezone

The objective of this operation is to determine at each time step the nodal velocities. This is done by simply extending to the two-dimensional case the dynamic rezone procedure used in References 9 and 10 for the propagation of planar flames.

In order to follow the flame front during its motion towards the fresh mixture, we move all the mesh points towards the cold boundary Γ_u with the same velocity $V(t) = [V(t), 0]$ at each time t. Therefore, between two static adaptations, everything happens as if the flame propagation were observed in a non-Galilean reference frame moving with the velocity $V(t)$. With such a procedure, the computational domain changes during the computation, but this is not a drawback since the problem (1)–(3) is posed on a semi-infinite domain. In the reference frame moving with the velocity $V(t)$, the grid and the computational domain D are fixed and the equations (1) become

$$T_t = \Delta T + \Omega(Y, T) + V(t) T_x, \tag{7a}$$

$$Y_t = \frac{1}{\mathrm{Le}} \Delta Y - \Omega(Y, T) + V(t) Y_x. \tag{7b}$$

At each time t, the velocity $V(t)$ is chosen in such a way that the integral of each of the variables T and Y in the computational domain D remains constant, i.e. $\int_D T_t = \int_D Y_t = 0$. Integrating (7a) and using the boundary conditions (4), we then get

$$\int_{\Gamma_b} T_x - \int_{\Gamma_u} T_x + \int_D \Omega(Y, T) + RV(t) = 0.$$

If the boundaries Γ_u and Γ_b are far enough from the flame front, the first two terms of this relation can be neglected to obtain the following expression for the mesh point velocities:

$$V(t) = -\frac{1}{R} \int_D \Omega(Y, T). \tag{8}$$

From a physical point of view, this is the expression of the instantaneous average flame speed at time t. Therefore, this very inexpensive dynamic rezone method is altogether adequate and efficient for our flame propagation problem: in the moving reference frame the flame front is deformed, but stays at the same place during the computation (see Figure 3). Moreover, the additional convective term $V(t)T_x$ in (7) allows the numerical solution of (7) to converge to a steady state instead of converging towards a travelling wave solution.

From a practical point of view, this dynamic rezone algorithm amounts to solving the problem (4)–(7) on a fixed grid. The time derivative, diffusive and reactive terms are discretized as in (6); for the convective terms, a finite-element formulation can be used (see (10) below), but the particular structure of the grid (which we now describe) also makes possible the use of a classical finite-difference formula.

Static rezone

The aim of the static rezone procedure is to compute a new adapted mesh, at a fixed time level, the current 'old' mesh and 'old' values of the variables being given. In our numerical study, this construction of an adaptive two-dimensional grid in the rectangle D is realized as follows.

We use a mesh whose data structure is intermediate between a logically rectangular two-argument grid $[x(i,j), y(i,j)]$ and a tensor-product grid $[x(i), y(j)]$: our mesh is divided into 'horizontal' straight lines parallel to the boundaries W and V and has the structure $N_{i,j} = [x(i,j), y(j)]$ (see Figure 6 below). Then it suffices for each line $y = y(j_0)$ to use a one-dimensional static rezone method for redistributing the nodes on this line. This will have the effect of concentrating many of the nodes N_{i,j_0} in the region where the wrinkled flame front crosses the line $y = y(j_0)$. For each horizontal line $y = y(j_0)$, we simply use the one-dimensional procedure developed in References 9 and 10 for planar flame propagation problems; this procedure does not change the total number of nodes. Once this is done, it remains to divide each quadrilateral $[N_{i,j}, N_{i+1,j}, N_{i+1,j+1}, N_{i,j+1}]$ into two triangles $[N_{i,j}, N_{i+1,j}, N_{i+1,j+1}]$ and $[N_{i,j}, N_{i+1,j+1}, N_{i,j+1}]$, which yields the new triangulation.

The new values of the variables at the new nodes are evaluated by interpolating the old solution on the old grid: for each straight line $y = y(j)$, this is again a one-dimensional procedure. We can use either a linear interpolation on each mesh of the old grid or a conservative interpolation.[11]

A few remarks should be added here. First, the distribution of the horizontal lines $y = y(j)$ is not modified during the computation (for the calculations reported below, these lines are equally spaced); obviously, their positions or their number could be evaluated using a one-dimensional adaptive procedure, although this would complicate the evaluation of the new solution. It should also be noticed that there is no coupling between the nodes on the line $y = y(j_0)$ and on the neighbouring lines $y = y(j_0 + 1)$ and $y = y(j_0 - 1)$.

Let us finally indicate briefly when this static rezone operation is used during the calculation (also see Reference 9 for more details on this question). The first static adaptation is performed after the initialization, before the first time step. Then, once a new grid has been computed at time t_0, another static rezone is realized only when the solution has been changing sufficiently since the last adaptation, i.e. when some norm of $U(t) - U(t_0)$ is greater than a given quantity (here U denotes the vector whose components are the values of the variables at the nodes). It can then be noticed that the number of static rezones performed per unit time (or per hundreds of time steps) decreases to zero when the numerical solution converges to a steady state.

REMARKS ON THE NUMERICAL METHOD

Stability criterion

Since an explicit time integration scheme is used for the numerical solution of (4)–(7), the value of the time step is to be chosen according to an appropriate stability analysis. Without presenting this analysis in detail, we simply sketch in this section the major point in the derivation of a stability criterion for the problem under consideration.

Such a stability analysis is easily carried out when classical finite-difference schemes are used on a uniform orthogonal mesh. For example, for a purely diffusive equation $u_t = \Delta u$, the stability analysis of the forward Euler scheme yields $\Delta t \leqslant \frac{1}{2}\Delta x^2$ in one space dimension and $\Delta t \leqslant \frac{1}{2}(\Delta x^{-2} + \Delta y^{-2})^{-1}$ on a two-dimensional orthogonal grid. However, compared to this simple case, several difficulties arise when investigating our problem (7): firstly because many more terms need to be considered and secondly because of the non-uniformity of the mesh. It appears in fact from several numerical experiments that a scheme operating with a certain time step may be stable on an orthogonal mesh and may become unstable on a non-orthogonal grid (the mesh sizes $\Delta x, \Delta y$ being held fixed). Therefore we need to take at least the non-orthogonality of the grid into account in our analysis. This can be done by comparing the non-orthogonal grid with a reference orthogonal grid: for instance, the regular non-orthogonal mesh A_1 represented in Figure 2 is the image of the regular orthogonal grid A_0 by the mapping $F(x, y) = (x', y') = (x + \delta y, y)$, where $\delta = \tan\gamma$. Then, solving $u_t = \Delta u = u_{x'x'} + u_{y'y'}$ on the grid A_1 amounts to solving $u_t = u_{xx} + u_{yy} - 2\delta u_{xy} + \delta^2 u_{yy}$ on A_0. The stability criterion of this last equation on the orthogonal mesh A_0 can easily be derived and gives $\Delta t \leqslant G(\delta)$ with, for instance, $G(0) = \frac{1}{2}(\Delta x^{-2} + \Delta y^{-2})^{-1}$ for the forward Euler scheme. This shows that the stability restriction for the equation $u_t = \Delta u$ on the non-orthogonal grid A_1 is of the form $\Delta t \leqslant G(\delta)$, in other words that the non-orthogonality of the grid does influence the stability analysis. Since we usually have $G(\delta) < G(0)$ for $\delta > 0$, we have explained why the time step restriction is more severe on non-orthogonal grids.

We do not give the exact expression of the stability criterion for the equations (7). But taking the non-orthogonality of the mesh into account in the stability analysis has been essential to allow successful explicit calculations even on adaptive non-orthogonal meshes with very obtuse angles (see Figure 6).

Evaluation of the grid velocity

As explained in the Dynamic rezone section, the grid point velocity $V(t)$ is obtained by imposing

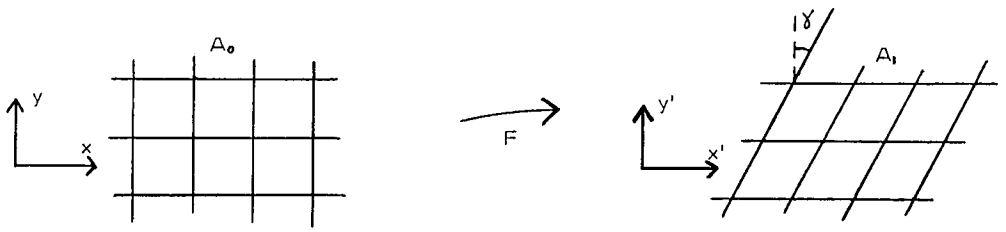

Figure 2. Transformation from an orthogonal to a non-orthogonal grid

a conservation property in the whole computational domain D: $\int_D T_t = \int_D Y_t = 0$. From a physical point of view, these relations mean that the thermal energy and the mass of reactant contained in the domain D are kept constant.

Thus, instead of using the value (8) of the grid velocity, it is interesting to stick to the conservation principle used to derive (8) and to try to impose the property $\int_D T =$ constant directly in the discrete scheme. Using the notations of the spatial approximation section, we can write the discrete expression of $\int_D T$ as $\sum_{j\in I} T_j \int_D \varphi_j$; we are therefore going to evaluate the grid velocity by imposing that this quantity remains constant during the calculation, i.e. by requiring

$$\sum_{j\in I} (T_j^{n+1} - T_j^n) \int_D \varphi_j = 0 \tag{9}$$

at all time steps (we use the superscripts $n, n+1$ to denote two consecutive time levels).

As explained above, the actual numerical scheme differs slightly from (6) because of the additional convective terms; assuming for simplicity that a forward Euler scheme is used for the time integration, we can write the discrete temperature equation as

$$\int_D \varphi_j \frac{(T_j^{n+1} - T_j^n)}{\Delta t} = -\int_D \nabla T_h^n \nabla \varphi_j + \Omega_j^n \int_D \varphi_j + V^n \int_D (T_h^n)_x \varphi_j \tag{10}$$

with $T_h^n = \sum_{i\in I} T_i^n \varphi_i$. Summing these equations for $j \in I^0$ and using (9), we get the following expression for the mesh velocity $V^n = V(t^n)$:

$$V^n = \frac{-\sum_{i\in I^0} \Omega_i^n \int_D \varphi_i + \int_D \nabla T_h^n \nabla \Phi}{\int_D (T_h^n)_x \Phi},$$

where $\Phi = \sum_{i\in I^0} \varphi_i$. Integrating the denominator by parts and using the boundary condition (4c)–(4d), we obtain finally

$$V^n = \frac{-\sum_{i\in I^0} \Omega_i^n \int_D \varphi_i + \int_D \nabla T_h^n \nabla \Phi}{R + \int_D T_h^n \Phi_x}. \tag{11}$$

This is the value of the grid velocity which we use in the discrete equations (10), whereas a straightforward discretization of (8) would have led to

$$V^n = \frac{-\sum_{i\in I} \Omega_i^n \int_D \varphi_i}{R}. \tag{12}$$

It is interesting to notice that the difference between (11) and (12) only consists of boundary terms since the function Φ is constant (and equal to 1) everywhere except in the neighbourhood of the boundaries Γ_u and Γ_b (this amounts to saying that the finite-element approximation of the diffusive and convective terms is conservative). In particular, the second term in the numerator of (11) corresponds exactly to the terms $\int_{\Gamma_b} T_x$ and $\int_{\Gamma_u} T_x$ which we have neglected in the derivation of (8).

The major reason for using (11) instead of (12) is the following: as already mentioned, one effect of our dynamic rezone method is to allow the solution to converge to a steady state. The expression (11), which guarantees the conservation property (9) up to round-off errors, will lead to a much

better convergence to steady state: for the first numerical example presented below, the use of (11) allows us to obtain residuals (i.e. $\max_{i \in I} |T_i^{n+1} - T_i^n| + \max_{i \in I} |Y_i^{n+1} - Y_i^n|$) less than 10^{-12}, while residuals of the order of 10^{-6} were obtained with the expression (12).

NUMERICAL RESULTS

We end this paper by presenting some results corresponding to physical situations where the planar flame is stable (we refer the reader to References 3 and 12 for an asymptotic stability analysis of the planar flame, and to References 1 and 2 for a numerical investigation of two-dimensional flame instabilities). More precisely, the numerical experiments whose results

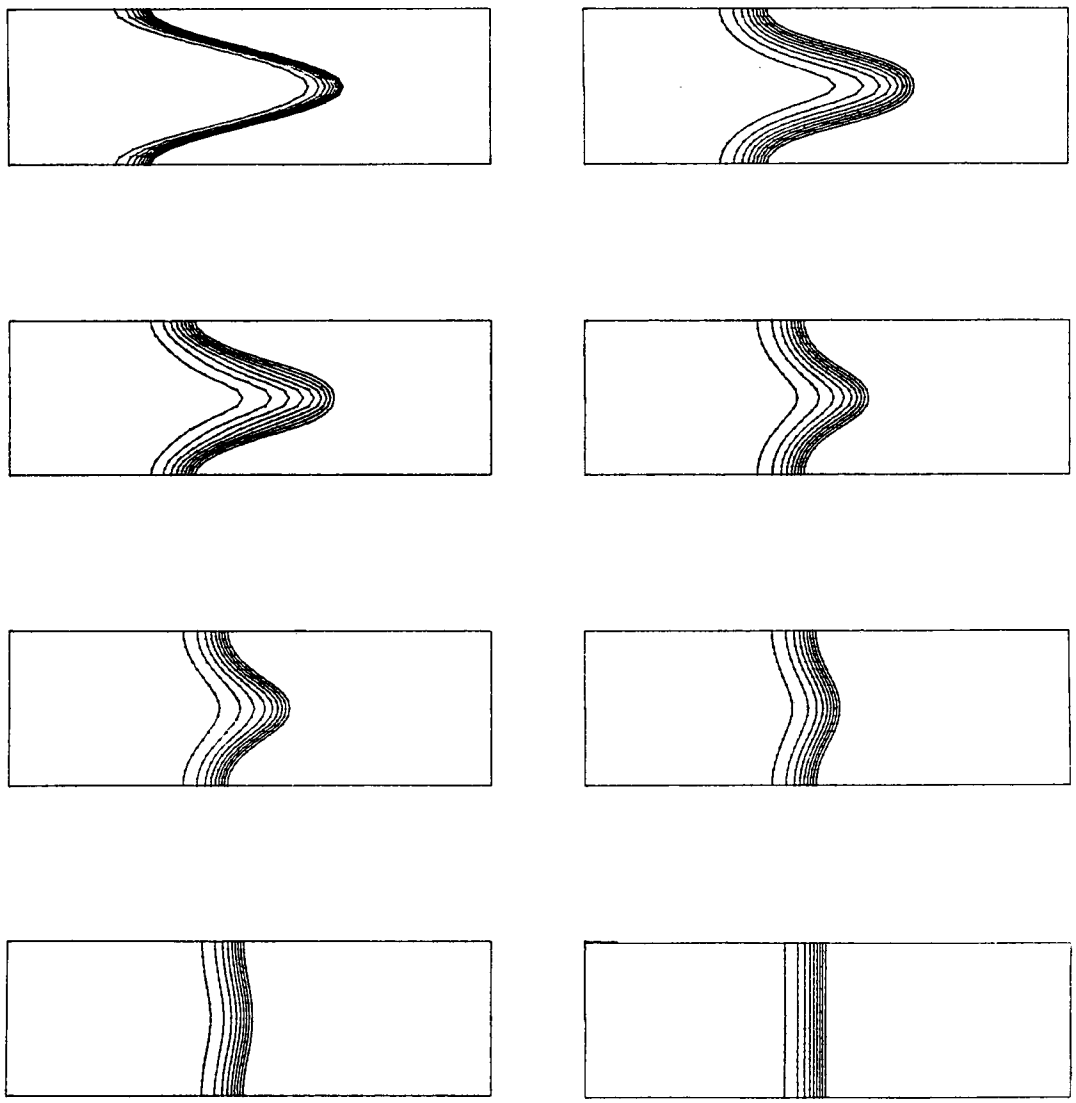

Figure 3. Adiabatic flame propagation: isotherms at eight successive time levels

are reported in this section have been carried out with the following values of the physical parameters: $\mathrm{Le} = 1, \beta = 10, \alpha = 0{\cdot}84$.

Figure 3 shows the adiabatic propagation of an initially wrinkled flame. The isotherms are plotted on the whole width of the tube, i.e. in the domain $E = [a, b] \times [-R, R] = \{(x, y), (x, y) \in D \text{ or } (x, -y) \in D\}$. One can observe that the wrinkled flame front converges to a planar steady state where all the isotherms are orthogonal to the tube walls, as expected from a physical point of view.

Figures 4 and 5 correspond to a different physical situation: the initially planar flame now tends

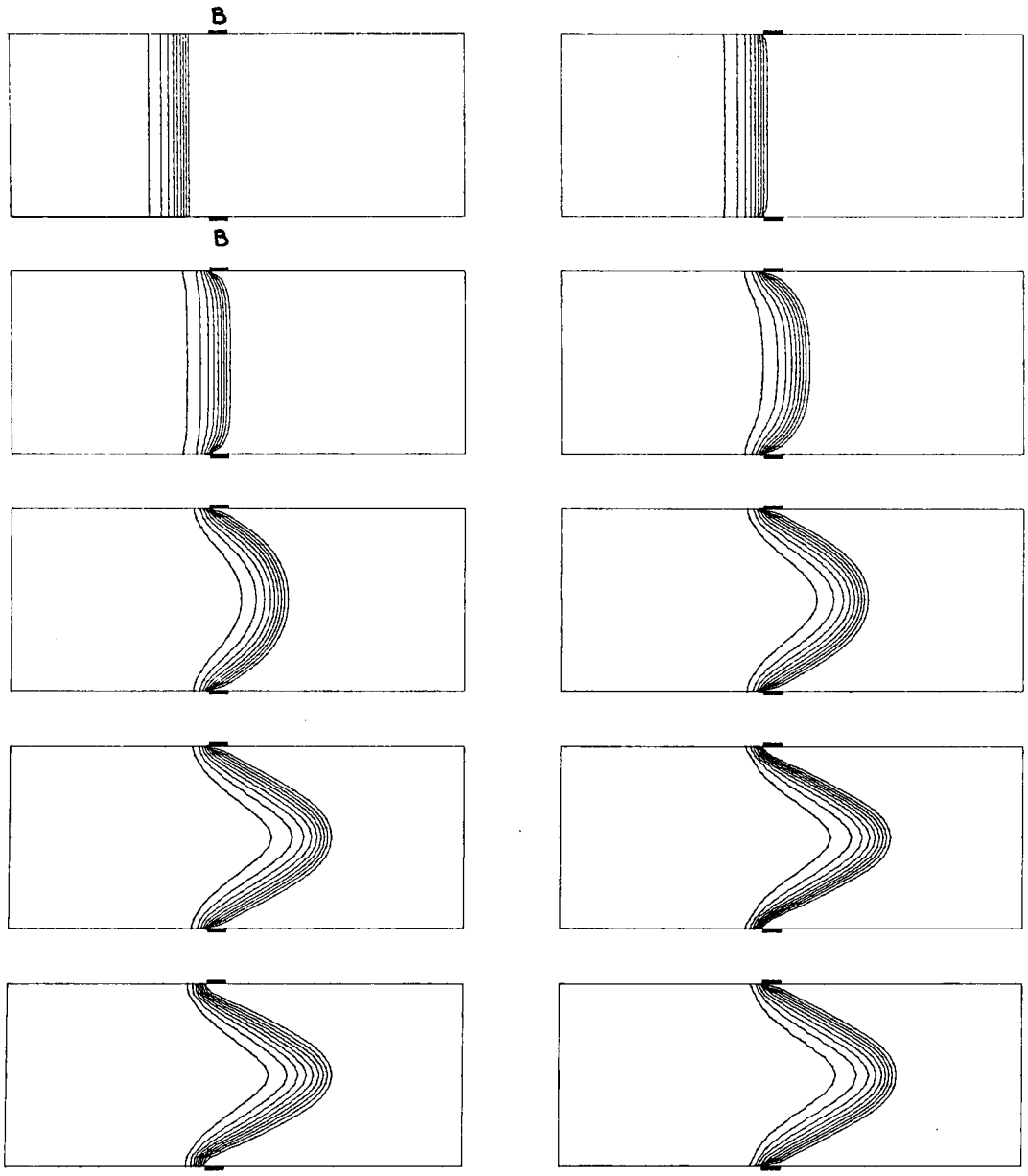

Figure 4. Non-adiabatic flame propagation: isotherms at ten successive time levels

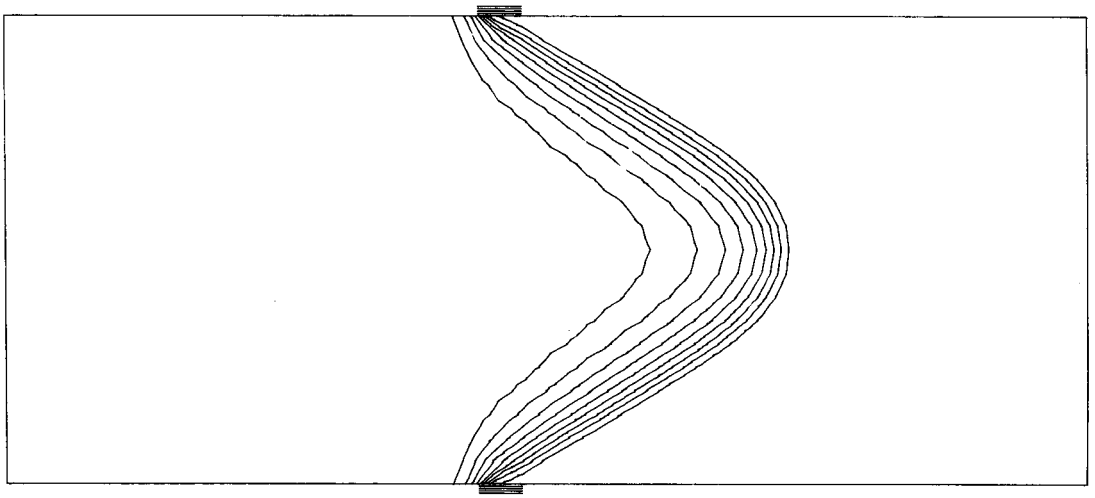

Figure 5. Non-adiabatic flame propagation: steady-state mass fraction contours

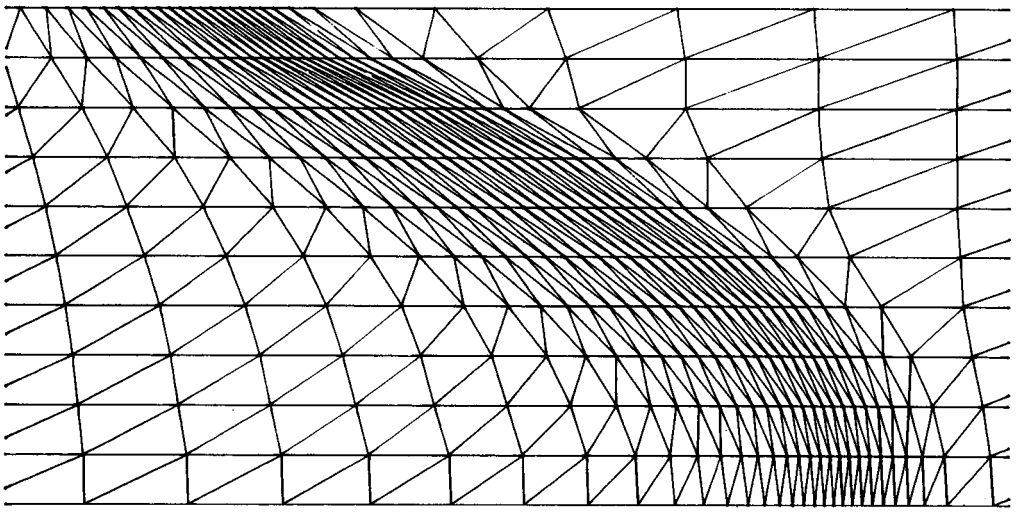

Figure 6. Blow-up of the triangulation near the flame front

to draw back towards the hot boundary (on the right) because a flow of fresh mixture is introduced at the left end of the channel, and a part B of the wall W is kept heated at the temperature $T_B = 1$. This non-adiabatic propagation is described by a slightly different set of equations:

$$T_t = \Delta T + \Omega(Y, T) + V_0 T_x,$$

$$Y_t = \frac{1}{\mathrm{Le}} \Delta Y - \Omega(Y, T) + V_0 Y_x,$$

where the velocity V_0 is now given and corresponds to a uniform gas flow in the tube (V_0 is to be chosen large enough so that the flame tends to propagate towards the right end of the tube). The boundary conditions (4) become

$$\frac{\partial T}{\partial n}=0 \quad \text{on} \quad W-\mathrm{B} \quad \text{and} \quad \text{on} \quad V,$$

$$T=1 \quad \text{on} \quad \mathrm{B},$$

$$T=0 \quad \text{on} \quad \Gamma_u, \quad \frac{\partial T}{\partial n}=0 \quad \text{or} \quad \Gamma_b,$$

for the temperature, and remain unchanged for the mass fraction. Notice that, in agreement with Remark 1, an homogeneous Neumann condition is to be used on Γ_b because the temperature of the hot gases is now unknown. The adaptive mesh strategy now simply consists of the static rezone procedure described earlier.

As observed on the figures, the heat source B behaves as a flame holder: the fresh mixture cannot cross this hot region without burning, and the flame front eventually converges to a wrinkled steady state shown in the last view of Figure 4 and in Figure 5. The finite-element triangulation of the computational domain D corresponding to this steady state is shown in Figure 6.

REFERENCES

1. F. Benkhaldoun, and B. Larrouturou, 'A finite-element adaptive investigation of two-dimensional flame front instabilities', to appear.
2. H. Guillard, B. Larrouturou and N. Maman, 'Numerical investigation of two-dimensional flame front instabilities using pseudo-spectral methods', to appear.
3. G. I. Sivashinsky, 'Instabilities, pattern formation, and turbulence in flames', *Ann. Rev. Fluid Mech.*, **15**, 179–199 (1983); see also 'Instabilities, pattern formation, and turbulence in flames', *Modélisation des Phénomènes de Combustion*, Eyrolles, Paris, 1985, pp. 121–204.
4. B. Larrouturou, 'The equations of one-dimensional unsteady flame propagation: existence and uniqueness', *SIAM J. Math. Anal.*, to appear.
5. N. Peters, 'Discussion of test problem A', in N. Peters and J. Warnatz (eds), *Numerical Methods in Laminar Flame Propagation, Notes in Numerical Fluid Mechanics*, **6**, Vieweg, Wiesbaden, 1982, pp. 1–14.
6. O. C. Zienkiewicz, *The Finite-element Method in Engineering Sciences*, McGraw-Hill, London, 1971.
7. J. A. Desideri and B. Larrouturou, 'Respecting consistency when combining finite elements and finite differences', *INRIA Report*, to appear.
8. F. Benkhaldoun and B. Larrouturou, 'Numerical analysis of the two-dimensional thermo-diffusive model for flame propagation', to appear.
9. B. Larrouturou, 'Utilisation de maillages adaptatifs pour la simulation de flammes monodimensionnelles instationnaires', in R. Glowinski, B. Larrouturou and R. Temam (eds), *Numerical Simulation of Combustion Phenomena, Lecture Notes in Physics*, **241**, Springer-Verlag, Heidelberg, 1985, pp. 300–312.
10. B. Larrouturou, 'Adaptive numerical methods for unsteady flame propagation', in G. S. S. Ludford (ed.), *Combustion and Chemical Reactors, Lectures in Applied Mathematics*, **24**(2), 1986, pp. 415–432.
11. B. Larrouturou, 'A conservative adaptive method for unsteady flame propagation', to appear.
12. J. D. Buckmaster and G. S. S. Ludford, *Theory of Laminar Flames*, Cambridge University Press, 1982.